PROCEEDINGS OF SCIENCE

The neutron structure function F_2 at high-x with BONuS at CLAS

Carlos Ayerbe-Gayoso, on behalf of the CLAS Collaboration[*†]
The College of William and Mary
E-mail: gayoso@jlab.org

The Barely Off-Shell Nucleon Structure (BONuS) experiment at CLAS12, at Jefferson Lab, will measure the neutron structure function F_2 for $0.1 < x < 0.8$ over a broad Q^2 range, from 1 to 14 GeV$^2/c$, using electron scattering from deuterium with spectator-proton tagging. By selecting the low-momentum recoil protons at large backward angles, final-state interactions as the deuteron breaks up can be minimized, and the deep-inelastic kinematics for the neutron can be determined. This technique, which has been used successfully at CLAS at 6 GeV, will be extended to a beam energy of 11 GeV with significantly increased luminosity. Details of the BONuS third generation Radial Time Projection Chamber and expected high-x F_2^n results are presented.

23rd International Spin Physics Symposium - SPIN2018 -
10-14 September, 2018
Ferrara, Italy

[*]Speaker.
[†]Run Group F at CLAS12

PoS(SPIN2018)030

1. Motivation

During the last 40 years, deep-inelastic lepton scattering off proton and nuclear targets ([1–4] and many others) have produced an accurate description of the proton structure function (SF) (Fig. 1 left), which is dominated by the u parton distribution function (PDF) as a function of the x-Bjorken:

$$\frac{F_2^p(x)}{x} = \left[\frac{4}{9}u(x) + \frac{1}{9}d(x)\right] \tag{1}$$

On the other hand, knowledge of the neutron SF is not well-known because the data are extracted from neutrons in bound nuclei, mainly from ^{2}H or ^{3}He. Such uncertainties are reflected in the extraction of the d PDF, which is the dominant term:

$$\frac{F_2^n(x)}{x} = \left[\frac{4}{9}d(x) + \frac{1}{9}u(x)\right] \tag{2}$$

A comparison of the difference in uncertainties is reflected in the figure 1 (right), showing the ratio of u (top) and d (bottom) to the CJ15 fit [5, 6] for different experimental PDF sets. Note that such uncertainties are even larger for $x \gtrsim 0.6$ where the $q\overline{q}$ sea contributions are negligible and the SF is dominated by the valence quarks.

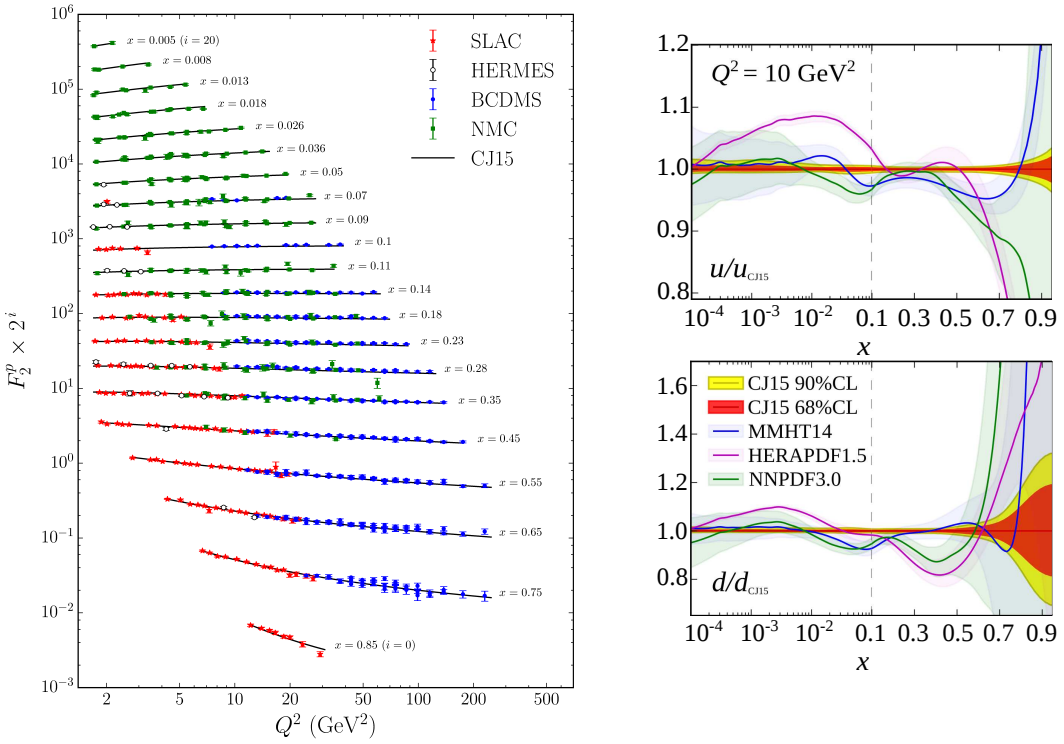

Figure 1: Left. Measured values of F_2^p together with the CJ15 fit, as a function of Q^2 at fixed x. The data have been scaled by a factor 2^i, from $i = 0$ for $x = 0.85$ to $i = 20$ for $x = 0.005$, and the PDF uncertainties correspond to a 90% C.L. **Right** Ratios of $u(x)$ (top) and $d(x)$ (bottom) to the CJ15. Note the different scales on the vertical axes showing the large uncertainties to the CJ15 fit on $d(x)$ for $x \gtrsim 0.6$ in comparison with the $u(x)$. (Ref. [6])

Several nucleon structure models, shown in table 1, predict the behavior of the ratio d/u as $x \to 1$ (eq. 3).

$$\frac{F_2^n(x)}{F_2^p(x)} \approx \frac{1+4d/u}{4+d/u} \Rightarrow \frac{d}{u} \approx \frac{4F_2^n/F_2^p - 1}{4 - F_2^n/F_2^p} \tag{3}$$

The ratio d/u as $x \to 1$ is also crucial for determining how the spin asymmetries A_1^n and A_1^p approach to $x \to 1$. Table 1 shows various model predictions that depend crucially on d/u at $x = 1$

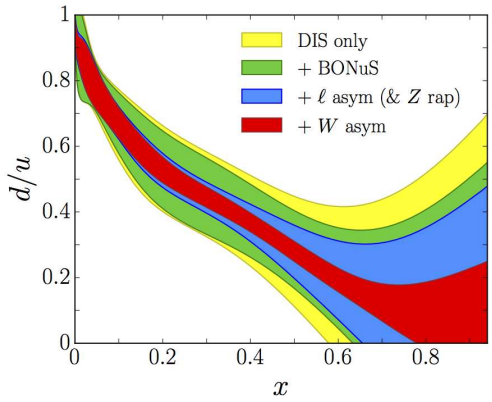

Figure 2: The ratio d/u uncertainties from different data sets (from [6]).

Model	d/u	A_1^p	A_1^n
SU(6)	1/2	5/9	0
pQCD	1/5	1	1
HSE	0	1	1

Table 1: d/u, A_1^p and A_1^nvalues at $x \to 1$ for representative nuclear models: SU(6) spin-flavour symmetry, perturbative QCD [7] and Hyperfine Structure Effect [8].

Neutron information from bound systems[1,2], mainly ^{2}H or ^{3}He, introduces several sources of uncertainty, Fermi motion, off-shell effects, final state interactions or the EMC effect influence the extraction [10–12]. However, model uncertainties, can be greatly reduced [14, 15]. The Barely Off-Shell Nucleon Structure (BONuS) experiment will make use of the spectator tagging method to determine F_2^n from deuterium. The method and the experiment are described next.

2. Spectator Tagging in the BONuS12 experiment

Energy conservation requires that the deuterium mass be the sum of the proton and the neutron energies: $E_p + E_n = M_d$. Because the mass of the deuteron is smaller than the mass of the proton plus the neutron, one or both nucleons must be off-shell. For certain kinematics, we can assume that the proton is a spectator and on-shell, while the neutron is off-shell with an $E^* = M_d - \sqrt{M_s^2 + p_s^2}$.

The final state motion of the spectator nucleon can be described by the light-cone fraction α_s:

$$\alpha_s = \frac{E_s - p_{s\|}}{M_s} \tag{4}$$

In the plane wave impulse approximation (PWIA) the recoiling proton momentum is equal and opposite to the neutron, thus the 4-momentum of the off-shell neutron is $p_n^\mu = (M_d - E_s, -\vec{p}_s)$, with M_d the mass of the deuterium nucleus. In the PWIA, the neutron is assumed to be on the energy shell, but off its mass shell, therefore the invariant mass of the free nucleon is:

[1] free neutrons decay in 15 min.

[2] ratio of typical proton target to magnetic neutron container [9] is $10^{17}:1$

$$M^{*2} = (M_d - E_s)^2 - \vec{p}_s{}^2 \tag{5}$$

In the same way, the Bjorken scaling variable $x = \frac{Q^2}{2M\nu}$ is replaced by:

$$x^* = \frac{Q^2}{2p_n^\mu q_\mu} = \frac{Q^2}{2\left((M_d - E_s)\nu + \vec{p}_s\vec{q}\right)} \tag{6}$$

Assuming $M_d \approx 2M$, $\vec{p}_s\vec{q} = p_{s\|}|\vec{q}|$, in the Bjorken limit $|\vec{q}|/\nu \to 1$, the light-cone fraction α_s, Equation 6 become:

$$x^* = \frac{Q^2}{2M\nu\left(2 - \frac{E_s - p_{s\|}(|\vec{q}|/\nu)}{M}\right)} \approx \frac{Q^2}{2M\nu(2-\alpha_s)} = \frac{x}{2-\alpha_s} \tag{7}$$

The total invariant mass of the hadronic final state in the $d(e,e'p_s)X$ reaction (see Figure 3):

$$\begin{aligned} W^{*2} &= (p_n^\mu + q^\mu)^2 = M^{*2} - Q^2 + 2(M_d - E_s)\nu + 2\vec{p}_s\vec{q} \\ &= M^{*2} - Q^2 + 2M\nu\left(2 - \frac{E_s - p_{s\|}(|\vec{q}|/\nu)}{M}\right) \\ &\approx M^{*2} - Q^2 + 2M\nu(2-\alpha_s) \end{aligned} \tag{8}$$

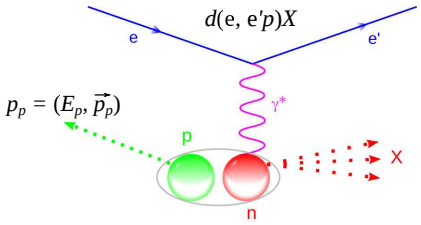

Figure 3: Diagram of the $d(e,e'p)X$ process. A high energy electron interacts with a deuterium nucleus through a virtual photon. The recoil proton is detected, ensuring that the virtual photon struck the neutron.

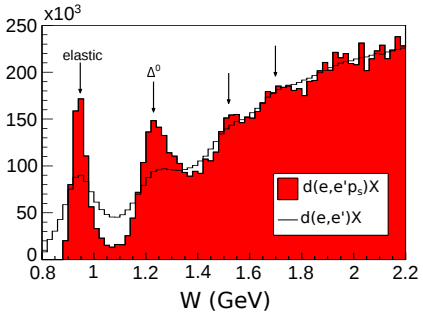

Figure 4: Invariant total mass spectra from inclusive scattering on deuterium compared (black line) with the tagged spectra (red area) showing the advantage of the method making the resonances to stand out [14]

.

The differential cross section with kinematics defined by the spectator-model values α_s and p_T can be calculated as:

$$\begin{aligned} \frac{d\sigma}{dx^* dQ^2} = \frac{4\pi\alpha_{EM}^2}{x^* Q^4}\left[\frac{y^2}{2(1+R)} + (1-y^*) + \frac{M^{*2}x^{*2}y^2}{Q^2}\frac{1-R}{1+R}\right] \\ \times F_2(x^*, \alpha_s, p_T, Q^2)\, S(\alpha_s, p_T)\frac{d\alpha_s}{\alpha_s} d^2 p_T \end{aligned} \tag{9}$$

in which $S(\alpha_s, p_T)\frac{d\alpha_s}{\alpha_s}d^2p_T$ is the probability of finding the spectator at p_T and α_s with the given kinematics, $R = \frac{\sigma_L}{\sigma_T}$ is the longitudinal to transverse cross section ratio, $y = \nu/E$ and $F_2(x^*, \alpha_s, p_T, Q^2)$ is the off-shell structure function of the struck neutron. Therefore $F_2^n = F_2(x^*, \alpha_s, p_T, Q^2) = F_2^{n\,\text{free}}(x, Q^2)$. Further details are given in Refs. [12, 13].

The method was used in the experiment E03-012 (BONuS) at Hall B at JLab in 2005 [14, 15]. A sample of the advantage of the method is presented in figure 4 showing the total invariant mass spectrum comparing the untagged spectra with the spectator tagged method. It is evident how the elastic and Δ^0 peaks improve their resolution and how the resonances stand out more clearly.

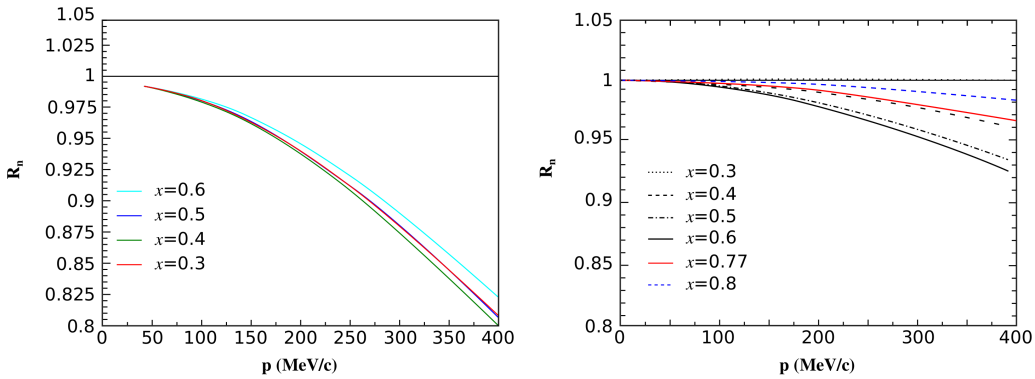

Figure 5: Off-shell effect dependence vs proton recoil momentum for different x values. **Left** from [16], shows that at 200 MeV/c the ratio is $\sim 5\%$ below the unity, and under 100 MeV/c that difference is $< 2\%$. **Right**, the model from [17] shows that at 200 MeV/c the ratio is $\sim 3\%$ below the unity, and below 100 MeV/c that difference is $< 1\%$.

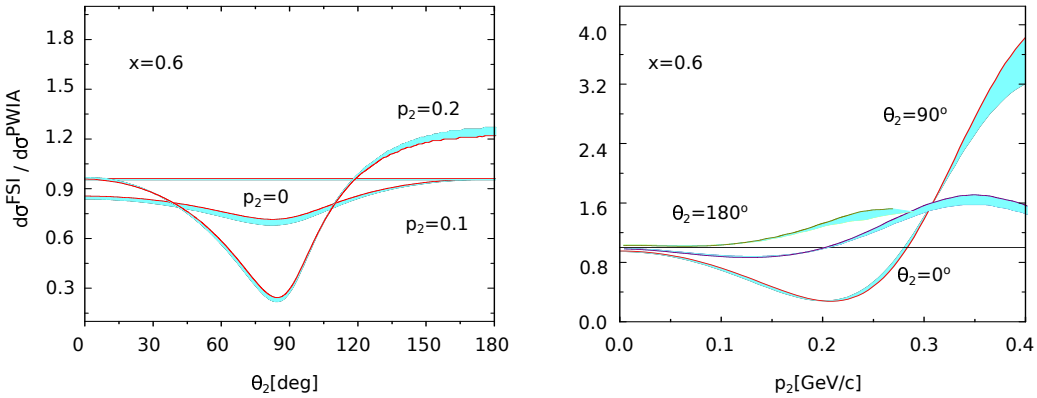

Figure 6: Final-state interaction model from [18]. **Left**, The FSI, PWIA ratio vs spectator proton angle for three different momenta (in GeV/c) at $x = 0.6$,. It shows that at very backward emission angles, the ratio difference from unity is practically negligible for protons at 100 MeV/c and $\sim 20\%$ for 200 MeV/c protons. **Right** FSI, PWIA ratio vs spectator proton momentum for three different emission angles at $x = 0.6$. It shows that the effect is reduced for low spectator proton momentum and specially at high backward angles.

The off-shell effects (the difference between the free neutron SF and the effective SF) were studied by different theory groups [16, 17], showing that selecting a very low momentum recoil

proton, the ratio $R_n \equiv F_2^{n(\text{eff})}/F_2^n$ differs from unity in less than 3%. Figure 5 shows two estimations of the off-shell effects using two different models.

Another possible source of uncertainty is the final state interaction (FSI), where the spectator proton interacts with deep inelastic remnants of the struck neutron. Several groups have calculated FSIs, demonstrating that backward-going spectators minimize such effect [18] (figure 6).

BONuS12 (JLab Experiment E12-06-113) at CLAS12 [19] will make use of the tagging spectator method, to determine $F_2^n(Q^2)$ for $0.1 < x < 0.8$, $1 < Q^2 < 14$ GeV$^2/c$, $W < 4.5$ GeV and Luminosity up to $2 \cdot 10^{34}$ cm^{-2} s^{-1}.

BONuS12 is expected to run 40 days at 11 GeV beam energy. To achieve this goal the standard CLAS12 equipment [20] is complemented with 3rd generation Radial Time Projection Chamber (RTPC), under development. Its description is given in the next section.

3. The BONuS12 RTPC

The BONuS12 RTPC is a gas detector in which the spectator proton produced in the $d(e,e'p)X$ reaction drifts due to the action of a radial electric field, and curves due to a longitudinal magnetic field produced by the solenoid in which the RTPC is embedded. The electrons produced by the ionization of the proton along its path, drift radially outwards and are amplified in 3 layers of GEM foils and registered with the readout system, then the scattered electron is measured by CLAS12.

The BONuS12 RTPC consists of a 40 cm long cylindrical chamber conformed by different concentric regions. At the center there is a target straw of 3 mm radius filled with Deuterium or Hydrogen at pressure of 7 atm. Next, there is a buffer region, filled with ^{4}He at 1 atm, to minimize the effect of Møller electrons, this region is surrounded by an aluminized mylar foil cylinder of 20 mm radius connected to the ground. The following two regions are filled by a mix of He and CO_2 at 1 atm in a proportion 80 -20% by volume. The regions are separated by a cylindrical aluminized mylar foil of 30 mm radius, acting as a cathode. A set of three GEM cylindrical foils will amplify the electron signal produced by the ionization of the gas in the drift region. The first GEM, with a radius of 70 mm, acts as the anode of the chamber, producing a radial electric field perpendicular to the beam. The second and third GEM foils have a radius of 73 and 76 mm respectively. Finally, a cylindrical printed circuit board with $\approx$ 18000 sensor pads collects the charged amplified by the GEMs. The whole chamber will be inserted in a solenoid which will produce a magnetic field parallel to the beam. Figure 7 shows a transverse scheme of the RTPC showing the different regions and the ionization process.

Each event contains the signal from all sensor pads integrated over 120 ns time intervals for a period of 2 μs before and 8 μs after the electron trigger signal from CLAS12, within the estimated maximum drift time, 5μs for the ionization electron to reach the GEMs. The read-out will be done through DREAM electronics [21] previously used in the Micromegas detector at CLAS12. It will allow BONuS12 a trigger rate $\sim$ 2kHz.

4. Expected results and Conclusions

BONuS12 expected results are summarized in the figure 8, comparing the estimated data results from the theoretical model from [22]. Selecting events with $W^* > 2$ GeV will allow to explore

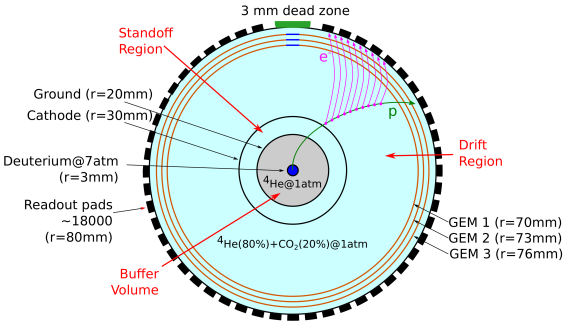

Figure 7: RTPC scheme showing the different concentric regions with a proton and the drifting electrons produced by the ionization of the proton in the gas.

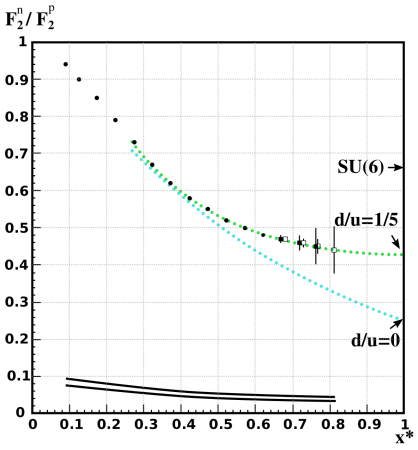

Figure 8: Expected F_2^n/F_2^p data points from BONuS12 12 comparing with the model from [22]. Dark symbols shows the expected results considering $W^* > 2$ GeV, having x^* up to 0.8. The open symbols are the expected data when using a "relaxed" cut, $W^* > 1.8$ GeV extending x^* up to 0.83. On the right axis different predictions to the d/u ratio are shown.

x^* up to 0.8. On the other hand, a relaxed cut of $W^* > 1.8$ GeV will extend x^* up to 0.83 and also improve the statistical uncertanty on lower x^* values.

BONuS12 will complement other experiments to determine the ratio d/u with different systematics like the MARATHON experiment at Hall A at JLab [23] comparing ^{3}He with tritium. MARATHON ran during the 2018 Winter/Spring beamtime and is under analysis. In the near future, the SoLID collaboration as part of the Parity-Violation in Deep Inelastic Scattering (PVDIS) experiment, plans to the measure the ratio d/u [24], estimating a 2% error over a range of x bins up to $x = 0.7$.

BONuS12 is scheduled to run in the first semester of 2020.

5. Acknowledges

The author would like to acknowledge the support from the Jefferson Science Associates, LLC through the JSA Junior Scientist Travel Support. Author work is supported by the DOE award DE-FG02-96ER41003.

References

[1] A. C. Benvenuti *et al.*, Phys. Lett. B **223**, 485 (1989); *ibid.* B **236**, 592 (1989)

[2] L. W. Whitlow *et al.*, Phys. Lett. B **282**, 475 (1992)

[3] M. Arneodo *et al.*, Nucl. Phys. B **483**, 3 (1997)

[4] A. Airapetian *et al.*, J. High Energy Phys. **05** 126 (2011)

[5] `https://www.jlab.org/theory/cj/`

[6] A. Accardi, L.T. Brady, W. Melnitchouk, J.F. Owens, N. Sato, Phys. Rev. D **93** 114017 (2016)

[7] G. R. Farrar and D. R. Jackson Phys. Rev. Lett. **35**, 1416 (1975)

[8] W. Melnitchouk and A. W. Thomas, Phys. Lett. B **377**, 11 (1996)

[9] S. Materne *et al.*, NIMA **611**, 2 (2009)

[10] Frankfurt and M. Strikman, Phys. Rep. 160, **235** (1988).

[11] W. Melnitchouk, M. Sargsian, and M. Strikman, Z. Phys.A 359, **99** (1997); M. Sargsian and M. Strikman, Phys.Lett. B 639, **223** (2006).

[12] S. Simula, Phys. Lett. B 387, **245** (1996).

[13] A.V. Klimenko *et al.*, Phys. Rev. C73 **035212** (2006)

[14] N. Baillie *et al.*, Phys. Rev. Lett 108, **142001** (2012), N. Baillie PhD Thesis, W&M (2010)

[15] S. Tkachenko *et al.*, Phys. Rev. C 89, **045206** (2014), S. Tkachenko PhD Thesis, ODU (2009)

[16] S. Liuti *et al.*, Phys. Lett. B 356(1995) **157**

[17] W. Melnitchouk *et al.*, Phys. Lett. B 335 **11** (1994) updated (2010)

[18] V. Palli *et al.*, Phys. Rev. C 80 (2009) **054610**

[19] S. Bueltmann, JLab PAC36 (2010)
`https://www.jlab.org/exp_prog/proposals/06/PR12-06-113.pdf`

[20] B.A. Mecking *et al.*, NIMA **503(3)** (2003)

[21] D. Attie *et al.* 19th IEEE-NPSS Real Time Conference (2014)

[22] F.E. Close, W. Melnitchouk, Phys. Rev. C68 **035210** (2003)

[23] G. G. Petratos, JLab PAC36 (2010)
`http://hallaweb.jlab.org/collab/PAC/PAC37/C12-10-103-Tritium.pdf`

[24] P. A. Souder, JLab PAC34 (2008)
`https://hallaweb.jlab.org/collab/PAC/PAC34/PR-09-012-pvdis.pdf`